



**HAL**  
open science

## Cellulose nanocrystal as ecofriendly stabilizer for emulsion polymerization and its application for waterborne adhesive

Ayman Ben Mabrouk, Alain Dufresne, Sami Boufi

► **To cite this version:**

Ayman Ben Mabrouk, Alain Dufresne, Sami Boufi. Cellulose nanocrystal as ecofriendly stabilizer for emulsion polymerization and its application for waterborne adhesive. *Carbohydrate Polymers*, 2020, 229, pp.115504. 10.1016/j.carbpol.2019.115504 . hal-03322772

**HAL Id: hal-03322772**

**<https://hal.science/hal-03322772>**

Submitted on 21 Jul 2022

**HAL** is a multi-disciplinary open access archive for the deposit and dissemination of scientific research documents, whether they are published or not. The documents may come from teaching and research institutions in France or abroad, or from public or private research centers.

L'archive ouverte pluridisciplinaire **HAL**, est destinée au dépôt et à la diffusion de documents scientifiques de niveau recherche, publiés ou non, émanant des établissements d'enseignement et de recherche français ou étrangers, des laboratoires publics ou privés.



Distributed under a Creative Commons Attribution - NonCommercial 4.0 International License

1 **Cellulose nanocrystal as ecofriendly stabilizer for emulsion polymerization and its**  
2 **application for waterborne adhesive**

3 Ayman Ben Mabrouk,<sup>a</sup>Alain Dufresne,<sup>b\*</sup> Sami Boufi<sup>a\*</sup>

4 <sup>a</sup> University of Sfax, Faculty of Science, LSME, BP1171-3018 Sfax, Tunisia

5 <sup>b</sup> Univ. Grenoble Alpes, CNRS, Grenoble INP, LGP2, F-38000 Grenoble, France

6 \* Corresponding authors: [alain.dufresne@pagora.grenoble-inp.fr](mailto:alain.dufresne@pagora.grenoble-inp.fr); [Sami.boufi@fss.rnu.tn](mailto:Sami.boufi@fss.rnu.tn)

7

8 **Keywords.** Cellulose; Nanocrystal; Nanocomposite; Emulsion polymerization; Waterborne  
9 adhesive.

10 **Abstract**

11 Soap-free emulsion polymerization of vinyl acetate (AVM) in the presence of cellulose  
12 nanocrystals (CNCs) was performed using persulfate/metabisulfite as initiator. The effect of the  
13 addition of MPEG comonomer on the locus of CNCs with respect to polymer particles was  
14 investigated. It was shown that the presence of MPEG strongly favors the accumulation of CNCs  
15 on the polymer particle thus contributing to a stabilization of polymer particle through Pickering  
16 effect. The rheological properties of the dispersion as well as the reinforcing effect of CNCs  
17 were also meaningfully affected by the presence of MPEG. For purpose of application, the  
18 polyvinyl acetate (PVA)/CNC nanocomposite dispersion was used as binder to produce PVA-  
19 based waterborne adhesive for wood. This open the way to produce high-value one pot  
20 nanocomposite dispersion ready for use, free from any surfactant likely to be used for  
21 waterborne adhesive or coating with higher mechanical performance.

## 22 INTRODUCTION

23 Nanocellulose has emerged as a new class of bio-based and sustainable nanomaterial derived  
24 from renewable resources with broad potential applications as highlighted in a number of recent  
25 reviews (Kargarzadeh, Mariano, Gopakumar, Ahmad, Thomas et al., 2018) and books (Dufresne,  
26 2017). Apart from being bio-based and renewable, nanocellulose is a water-based product  
27 produced without using harmful chemicals and organic solvents. The technology for its  
28 production is scalable and its commercial production has recently been launched by several  
29 companies and start-ups with a world production expected to total about \$300 billion dollars by  
30 2030 (<https://www.gminsights.com/industry-analysis/nanocellulose-market>).

31 Nanocellulose encompasses cellulose nanofibrils (CNFs), bacterial cellulose (BC) and cellulose  
32 nanocrystals (CNCs). The difference among the three classes of nanocellulose is mainly their  
33 morphology and method of production. The stiff form of CNC along with their elementary  
34 crystallite form gives rise to remarkable mechanical properties with an axial elastic modulus in  
35 the range of 110-180 GPa (Eichhorn, 2012) and strength around 2-3GPa (Saito, Kuramae,  
36 Wohler, Berglund & Isogai, 2013). These outstanding mechanical properties of CNC justify the  
37 focus on embedding CNC into a polymer to reinforce the mechanical properties of the material.  
38 The expected benefits from this association are: 1) increase in stiffness as well as strength, 2)  
39 preservation of optical properties of the polymer and density, and 3) better resistance to solvent  
40 and to deformation under heat. However, given their nanoscale, high specific surface area,  
41 hydrophilic character and strong tendency to self-aggregate through hydrogen bonding, the  
42 dispersion of CNCs within a polymer matrix, especially hydrophobic one, is not straightforward,  
43 resulting in poor-quality nanocomposites. This justifies that conventional melt processing route  
44 for CNC-based nanocomposite cannot be used without surface modification of the nanofiller.  
45 Mixing CNC suspension with polymer in the form of aqueous dispersion followed by casting and

46 film-formation process revealed to be the most efficient route to benefit from the strong  
47 reinforcing effect of CNC, likely due to high degree of individualization of CNCs promoting the  
48 set-up of a percolated CNC network held through hydrogen bonding, which is of key importance  
49 in the reinforcing mechanism (Boufi, Kaddami & Dufresne, 2014).

50 Waterborne polymer dispersions are becoming increasingly important with broad industrial  
51 applications in paint and coating, adhesives, building and construction, paper and board among  
52 others. Emulsion polymerization is the most employed method for the synthesis of polymer  
53 dispersions offering the possibility of numerous advantages (Chern, 2006) including low  
54 viscosity while keeping a high molecular weight, facility to scale-up without high investment,  
55 relatively high reaction rate, and environmental friendliness due to the use of water.

56 As mentioned, the addition of CNCs with contents up to 10-15 wt% to a polymer dispersion is a  
57 convenient way to strongly enhance the stiffness and the strength of the film in the rubbery  
58 domain. In waterborne adhesive, the addition of CNCs results in an enhancement of shear  
59 strength, tack, and peeling strength for pressure sensitive adhesive (PSA) (Dastjerdi et al., 2018),  
60 and in bonding strength for PVA based adhesive (Kaboarani, Riedl, Blanchet, Fellin, Hosseinaei  
61 et al., 2012).

62 For easier use of CNC as reinforcing additive in polymer dispersion, the in-situ polymerization  
63 techniques, where the CNC suspension is mixed with monomer prior to polymerization would be  
64 preferred to the ex-situ mixing route. The former approach would deliver single nanocomposite  
65 dispersion ready for use without necessity of an intermediate mixing step requiring appropriate  
66 dispersion tool. Moreover, the in-situ synthesis is expected to contribute to intimate contact  
67 between nanocellulose and polymer particle through physical interaction but also covalent  
68 bonding during the polymerization process. The presence of nanocellulose might also contribute  
69 to the stabilization of the polymer dispersion through Pickering effect, in which nanocellulose

70 adsorbed on the surface of the polymer particle generates a physical barrier impeding the particle  
71 from aggregation. Recent literature data dealing with in-situ emulsion polymerization of  
72 nanocellulose for adhesive and coating application is cited in the following. Pressure sensitive  
73 adhesive (PSA) films were prepared by in-situ semi-batch emulsion polymerizations using  
74 isobutyl acrylate, n-butyl acrylate, and methyl methacrylate in the presence of CNCs with  
75 loading levels up to 1 wt% (Ouzas, Niinivaara, Cranston & Dubé, 2018a; Dastjerdi, Cranston &  
76 Dubé, 2017). Improvement in tack, peeling strength and shear strength for the PSA films was  
77 pointed out. Similar work was reported by (Yu, Yang, Wang, Dong, Du et al., 2019) where  
78 acrylic PSA nanocomposite reinforced with CNC was successfully synthesized by in-situ  
79 emulsion polymerization of acrylic monomer in the presence of CNC grafted with 3-  
80 methacryloxypropyltrimethoxysilane without addition of surfactant. CNC armored latex particles  
81 directly by emulsion polymerization using cationic initiator was reported by (Limousin, Ballard  
82 & Asua, 2019) using a cationic initiator to promote the adsorption of the negatively charged  
83 CNCs onto the latex particle surface. Zhou et al. have reported the synthesis of soap-free  
84 emulsion fluorinated polyacrylate via reversible addition-fragmentation chain-transfer  
85 polymerization (RAFT) assisted Pickering emulsion polymerization using CNC modified with  
86 poly(2-(dimethylamino) ethyl methacrylate)-*b*-poly(glycidyl methacrylate)-*b*- (Zhou, Li, Li &  
87 Yao, 2019). Most of the published literature data pointed out a beneficial effect of the presence  
88 of nanocellulose during the in-situ radical dispersion polymerization. However, the number of  
89 published paper focusing on this topic remains low when compared to the abundant literature on  
90 cellulose nanocomposites. In view of the promising results reported in these recent papers,  
91 additional work is needed to further highlight the beneficial effect of the presence of  
92 nanocellulose during in-situ radical dispersion polymerization.

93 In the present work we pursue our investigation concerning the impact of the presence of  
94 nanocellulose during in-situ emulsion polymerization in the absence of any added surfactant.  
95 Polyvinyl acetate dispersion was prepared by emulsion polymerization in the presence of CNCs  
96 and without any added surfactant. The main emphasis was put on how the addition of  
97 polyethylene glycol methacrylate (MPEG) comonomer at low level affected the colloidal  
98 properties of the dispersion and the reinforcing potential of CNCs. Finally, application of PVA-  
99 CNC latex dispersion as adhesive for wood was evaluated.

## 100 **MATERIAL AND METHODS**

### 101 **Materials**

102 Vinyl acetate (VAM), potassium persulfate (KPS), sodium metabisulfite and polyethylene glycol  
103 methacrylate ( $M_n = 375 \text{ g}\cdot\text{mol}^{-1}$ ) (MPEG) were supplied by Aldrich and used without further  
104 purification. Distilled water was used for all the polymerization and treatment processes.

105 ***Preparation of cellulose nanocrystals.*** The preparation of cellulose nanocrystals from alfa fibers  
106 was classically carried out by acid hydrolysis acid approach. The method used to prepare CNC  
107 was reported elsewhere (Mabrouk, Kaddami, Boufi, Erchiqui & Dufresne, 2012). Briefly, 1000  
108 mL of an aqueous solution of  $\text{H}_2\text{SO}_4$  at 65% by mass was poured into a beaker and placed in a  
109 water bath at  $45^\circ\text{C}$ . After stabilization of the temperature of the solution, 50 g of bleached and  
110 dry alfa fibers was added. Then, the dispersion was homogenized by mechanical stirring for 30  
111 min. The role of the acid is to dissolve the amorphous phase of cellulose to release cellulose  
112 nanocrystals which are well dispersed in water and isolated from each other by the intermediary  
113 of sulfate ions present on their surface. After 30 min of hydrolysis, the CNC suspension is  
114 centrifuged in order to remove most of the acid. Dialysis against distilled water was performed to  
115 remove free acid in the dispersion. This was verified by neutrality of the dialysis effluent.  
116 Complete dispersion of the nanoparticles was obtained by a sonication step.

117 **Emulsion polymerization.** The recipe for the emulsion polymerization of VAM in the presence  
 118 of CNCs is given in Table 1. The procedure adopted is the following: CNC was first dispersed in  
 119 appropriate volume of water so that the whole amount of water was 17 mL, and was sonicated for  
 120 2 min at 70% amplitude (Sonics Vibracel Model CV33) to ensure effective dispersion. Then,  
 121 VAM was added and gently emulsified by stirring using a magnetic stir bar for several min to  
 122 create a coarse monomer emulsion, and finally the mixture was flushed with N<sub>2</sub> to remove  
 123 trapped O<sub>2</sub>. When the polymerization was carried out in the presence of MGEG, the co-monomer  
 124 was added in the water phase containing CNCs. The polymerization was triggered by raising the  
 125 temperature to 50°C and the addition of KPS (initiator)/Na<sub>2</sub>S<sub>2</sub>O<sub>5</sub> in water (redox activator)  
 126 separately during 2h. Polymerization was completed within 4-5h and the completing of the  
 127 polymerization was checked by measuring the solid content. All the polymerization runs were  
 128 carried out at 15 wt% solid content.

129 **Table 1.** Recipe for the emulsion polymerization of vinyl acetate in the presence of CNC without  
 130 any added surfactant (amounts in g).

Component	Composition
Water	17
VAM	3
KPS	0.1
Na <sub>2</sub> S <sub>2</sub> O <sub>5</sub>	0.1
MPEG	0/0.15
CNC	0 to 0.3
Temperature (°C)	60

131

132 **Preparation of nanocomposite films.** Nanocomposite films were prepared by casting the  
133 nanocomposite dispersion in a Teflon mold and storing at 40-50°C for several hours until  
134 complete evaporation of water and film-formation process. A transparent to translucent film with  
135 thickness in the range of 300-400 µm was obtained. The thickness of the film was measured  
136 using electronic digital gauge meter.

### 137 **Characterization methods**

138 **Particle size.** The average diameter of polymer particles was determined using dynamic light  
139 scattering (Malvern Zetasizer Nano S, Malvern Instruments Ltd., Malvern, UK). The sample was  
140 diluted 10 times. Each measurement was repeated three times, and the average value was  
141 retained as the particle size.

142 **ζ-potential.** ζ-potential values were measured at 25°C using a laser Doppler electrophoresis  
143 apparatus (Malvern Nano-Zetasizer ZS, UK). The sample was diluted with KCl solution (to  
144 buffer the ionic strength) to about 0.01 wt% of polymer particles. The measurements were  
145 performed three times for each sample.

146 **Field-emission scanning electron microscopy (FE-SEM).** FE-SEM was performed at the  
147 CMTc characterization platform of Grenoble INP using a ZEISS Gemini SEM 500 Field-effect  
148 scanning electron microscope. A drop of the diluted nanocomposite dispersion (with a solid  
149 content of 0.1 wt%) was deposited on a surface of a silicon wafer and lyophilized to remove  
150 water without any risk of polymer particle or CNC aggregation. Then, the sample was coated  
151 with a thin layer of Pt applied by sputtering with a thickness limited to about 1 nm.

152 **Atomic force microscopy (AFM) observation.** An atomic force microscope (AFM) (Flex AFM  
153 from Nanosurf) was used to examine the morphology of CNC. Analyses were performed in  
154 tapping mode at a vibration frequency 130 KHz and vibration amplitude 150mV. The samples

155 were prepared by depositing a drop of diluted CNC suspension (with a solid content about 0.01  
156 wt%) on the surface of a silicon wafer and leaving it to dry for 1h.

157 ***Rheological Measurements.*** The rheological properties of latex dispersions were measured  
158 using a stress-controlled rheometer (Kinexus Pro+, Malvern Instruments, UK) with a cone plate  
159 geometry (cone angle, 2°; diameter, 20 mm; truncation, 56 µm) at 25°C. Steady-state viscosity  
160 investigation was performed in a shear rate range from 0.01 to 10 s<sup>-1</sup>. Strain sweep measurements  
161 were performed within a strain range from 0.01% to 100% at a fixed frequency of 1 Hz.

162 ***Dynamic mechanical analysis (DMA).*** DMA experiments were carried out with a PYRISTM  
163 Diamond DMA (Perkin-Elmer, Waltham, MA), working in tension mode. Samples were heated  
164 from -30 °C to 120 °C with a heating rate of 3 °C.min<sup>-1</sup> at a frequency of 1 Hz and amplitude of  
165 10 µm. The storage (*E'*) modulus was measured as a function of temperature. Sample dimensions  
166 were about 20 mm (length) by 7 mm (width) and 0.2 mm (thickness).

167 ***Differential scanning calorimetry (DSC).*** DSC measurements were carried out using a Perkin-  
168 Elmer Pyris Diamond DSC under nitrogen flow from -50 °C to 120 °C, with a heating rate of  
169 10°C.min<sup>-1</sup>. The *T<sub>g</sub>* values were measured during the second temperature sweep.

170 ***Transmittance measurements.*** The transmittance of the nanocomposite films was measured  
171 between 700 nm and 400 nm using UV-Vis Spectrometer Lambda 35 (Perkin Elmer, USA.) in  
172 transmittance mode.

173 ***Fabrication of adhesive and tests of wood joints.*** PVA based adhesive was prepared by mixing  
174 10g of the PVA dispersion with 5 g of polyvinyl alcohol solution (Selvol PVOH 508) at 10%  
175 concentration. The bond strength of the adhesive was tested by preparing specimens of wood  
176 joints following NF EN 205 standard. The specimen of wood was cut into (150×20×5) mm, was  
177 glued with the adhesive, compressed under a static pressure of 1MPa at room temperature for 2h

178 and then conditioned at 25°C and 50% relative humidity (RH) for 7 days to ensure equilibrium  
179 moisture content and effective drying of the adhesive joint.

180 The bond strength was tested in a tensile test machine and the shear strength  $T$  ( $\text{N}\cdot\text{mm}^{-2}$ ), was  
181 calculated by using Eq. 1. The measurements were replicated five times for each sample and  
182 average values were reported.

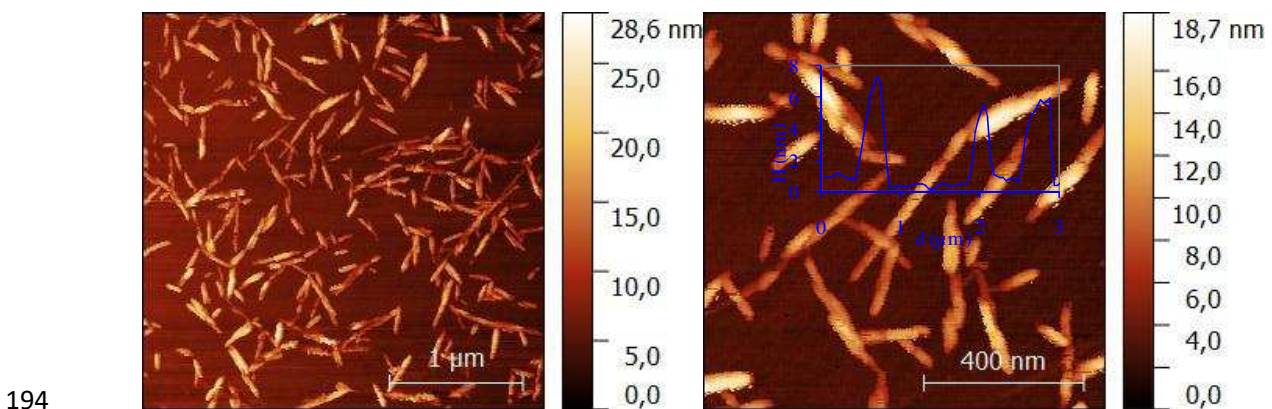
183 
$$T = \frac{F_{\max}}{lB} \quad (\text{Eq. 1})$$

184 Where  $F_{\max}$  is the maximum force at break (N),  $B$  is the width of tested bonded surface (mm),  
185 and  $l$  is the length of tested bonded surface (mm).

## 186 RESULTS AND DISCUSSION

### 187 Characterization of CNC

188 CNCs used in the present work were produced from bleached alfa fibers following the well-  
189 known sulfuric acid hydrolysis route. The as-produced CNCs have a needle-like morphology  
190 with an average length around  $250 \pm 20$  nm and average width of  $10 \pm 2$  nm, based on AFM  
191 observations (Figure 1). The CNCs were negatively charged over the whole pH range from 2 to  
192 12 with a  $\zeta$ -potential value around -40 mV, which is expected given the presence of sulfate ester  
193 groups remaining fully ionized over the whole pH range.



195 **Figure 1.** AFM height images for CNCs at two magnifications and cross section height profile  
196 (inset).

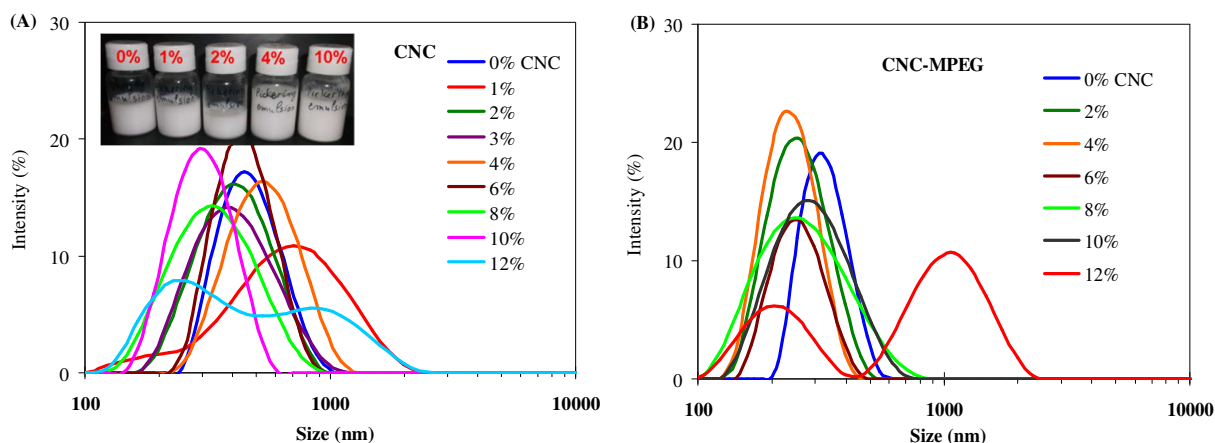
### 197 **Emulsion polymerization of VAM in the presence of CNCs**

198 Emulsion polymerization of VA was carried out in batch mode by gentle mixing of the monomer  
199 with the CNC suspension at a concentration ranging between 2 and 12 wt% based on the VA  
200 content, without addition of neither any surfactant nor any co-stabilizer. The polymerization was  
201 activated by adding KPS/SMB separately during 2h at a temperature of 50°C. Except for  
202 polymerization conducted in the presence of 1 and 12 wt% CNC, all the ensuing PVA  
203 dispersions were white-aspect emulsion (see photo in the inset of Fig. 2A) free from any  
204 coagulum. The particle size distribution of the PVA-CNC nanocomposite dispersion determined  
205 from DLS measurement is shown in Figure 2A. For dispersions with CNC content ranging from  
206 2 to 10 wt%, a monomodal distribution is observed with mean particle size ranging from 300 to  
207 500 nm and the dispersion remained stable over 6 months storage at room temperature. At 1 and  
208 12 wt% CNC loading, two populations of polymer particle could be seen, peaking at 200 /800nm  
209 and 250/900 nm, respectively. The presence of particles with size exceeding 1000 nm could  
210 explain the settling of the PVA/CNC emulsion when stored for 2-3 weeks since the effect of  
211 gravity of polymer particle cannot be overcome by Brownian motion. On the other hand, for  
212 CNC contents between 2 and 10%, the particle size is below 500 nm and the dispersion remained  
213 stable due to the presence of negative surface (negative zeta potential exceeding 25 mV) bringing  
214 enough electrostatic stabilization effect to avoid aggregation.

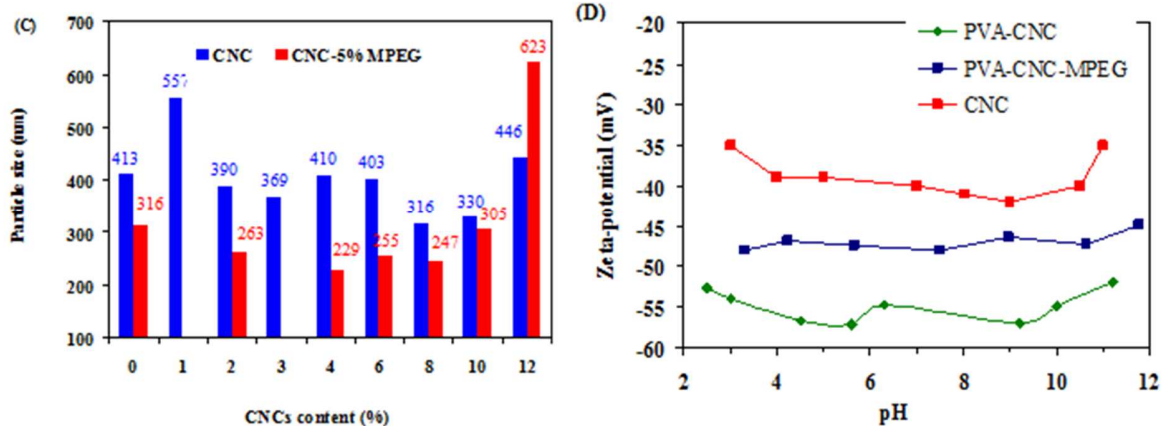
215 The evolution of the mean particle size vs CNC content doesn't reveal any clear trend about the  
216 effect of CNC on the size of the nanocomposite dispersion. The particle size of the dispersion  
217 attained about 500-600 nm for the PVA dispersion produced without CNC and 1 wt% CNC and

218 then decreased to about 350-400 nm remaining roughly the same as the CNC content is ranging  
219 between 2 and 10 wt%. This means that CNCs contribute only partially to the stabilization of the  
220 polymer particle without being an effective Pickering stabilizer for polymer particles. Indeed, in  
221 Pickering effect, where solid particles replace surfactant molecules to impart colloidal  
222 stabilization, a close dependence between the particle size of the dispersion and the solid particle  
223 content is observed with a diameter decreasing in an inversely proportional rule with the solid  
224 particle content. This correlation is expected assuming that solid particle needs to be attached to  
225 the oil droplet to ensure stabilization and the increase in the solid particle content brought higher  
226 available interfacial area to cover the dispersed organic phase. However, the presence of CNCs  
227 with contents between 2 to 10 wt% (with respect to monomer) during the emulsion  
228 polymerization did alter neither the particle size nor the stability of the dispersion. The poor  
229 stabilization capacity of CNCs in Pickering emulsion polymerization of VAM could be  
230 explained by the highly hydrophilic character of CNCs along with the presence of sulfate  
231 charged groups on the surface of CNCs. Accordingly, the cellulose nanoparticles will  
232 preferentially accumulate within the continuous water phase and only a fraction of CNCs are  
233 likely to adsorb on the polymer particle during their nucleation and growth, without being able to  
234 ensure high coverage degree which is prerequisite for effective Pickering stabilization process.  
235 This hypothesis could be confirmed by FE-SEM observation revealing the presence of free  
236 CNCs nearby polymer particle after removal of water by freeze-drying to freeze the structure of  
237 the dispersion (see Fig. 3).

238



239



240 **Figure 2.** Particle size distribution of the PVA dispersion prepared (A) in the presence of CNC,  
241 (B) CNC-5%MPEG; (C) mean particle size vs CNC content, and (D) Zeta-potential of the  
242 dispersion vs pH.

243 Aiming to reduce the particle size of the PVA polymer latex and further promote the stabilization  
244 process, the emulsion polymerization of VAM in the presence of CNCs was performed in the  
245 presence of MPEG used as co-monomer. Results shown in Figure 2B pointed out a systematic  
246 decrease in the particle size in the presence of MPEG. This co-monomer is known to improve the  
247 freeze-thaw stability thanks to the presence of polyethylene glycol chains covalently bound to  
248 the polymer particle, providing steric stabilization without any risk of detachment from the

249 surface. Presently, it can be seen that emulsion polymerization performed in the presence of  
250 MPEG and CNC led to stable polymer dispersions with size ranging from 220 to 280 nm over  
251 CNC contents between 2 to 8 wt%. The decrease in the particle size when CNCs were present  
252 during the polymerization process is indicative of a synergetic effect between MPEG and CNC,  
253 reinforcing the stabilization process, presumably by favoring the attachment of CNCs to the  
254 polymer particles. The possibility of adsorption of PEG chains on CNC has been highlighted in  
255 the literature (Cheng, Wen, Wang, An, Zhu et al., 2015; Sheibat-Otman & Bourgeat-Lami,  
256 2009).

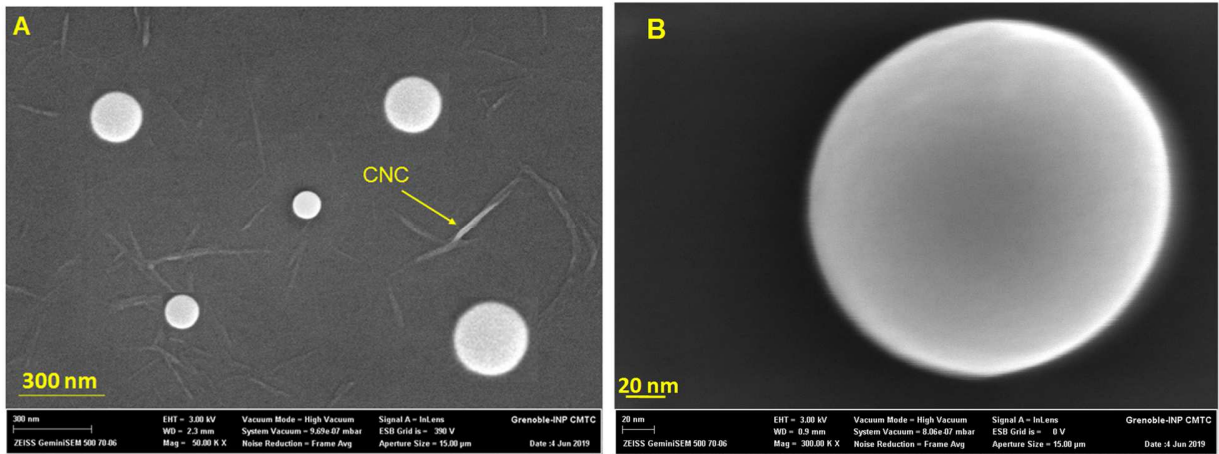
257 One might wonder if the presence of MPEG is likely to affect the interfacial tension that might  
258 contribute to the better stabilization effect in its presence. To investigate this issue, surface  
259 tension and zeta-potential measurements were carried out on latex dispersions prepared via  
260 Pickering emulsion polymerization in the presence of 8% CNCs with and without MPEG. The  
261 surface tension attained 61 and 53 mN.m<sup>-1</sup> for latex at 8% CNC synthesized in the absence and in  
262 the presence of MPEG, respectively. However, prior to the polymerization reaction, the surface  
263 tension was found to be around 41 mN.m<sup>-1</sup> when MPEG was present. The increase in the surface  
264 tension after polymerization is presumably due to the consumption of MPEG by  
265 copolymerization with AVM. The reduction in surface tension observed before polymerization  
266 when MPEG was present might also contribute to enhance the stability of the emulsion and of  
267 the latex dispersion.

268 It is worth noting that prior to the activation of the polymerization reaction, the emulsion has a  
269 broad particle size distribution encompassing population with micros size droplet spanning from  
270 700 nm to several  $\mu\text{m}$  and nanoscale particles with size lower than 100 nm (Figure S1 in  
271 Supplementary Material). In the absence of CNC and MPEG, the emulsion was unstable and  
272 phase separation occurred instantaneously with creaming of the monomer on the top of the water

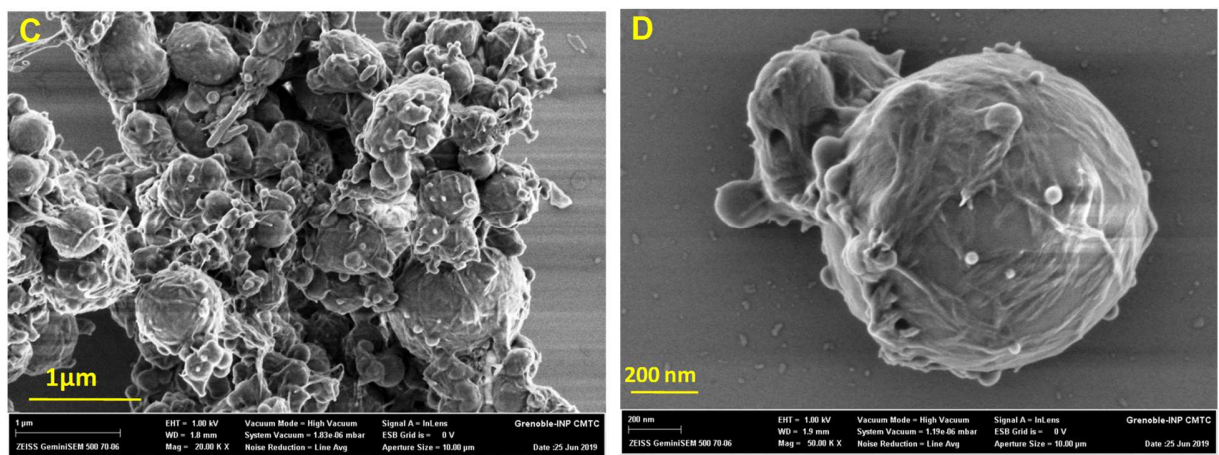
273 phase. In the presence of CNC the emulsion remained stable up to 6h and a shift to lower particle  
274 size distribution was observed with increasing CNC contents, indicating an enhancement in the  
275 emulsion stability, which is in agreement with literature data (Kalashnikova et al., 2013). For the  
276 same CNC content, the addition of MPEG further decreased the particle size of the emulsion  
277 which is likely due to the surface activity of MPEG brought by polyethylene glycol segment in  
278 MPEG. However, when compared to the PVA-CNC latex dispersion, the particle size is much  
279 higher and coarser, which further confirmed that the polymerization reaction took place via  
280 emulsion polymerization route.

281 The  $\zeta$ -potential value of the dispersion remained nearly the same around -50 to -55 mV and did  
282 not change considerably over the whole CNC content from 1 to 12 wt% (Fig. 2D). The higher  
283 value of  $\zeta$ -potential (in absolute value) for the nanocomposite dispersion is indicative of polymer  
284 particles having higher surface charge density than CNCs. These negative charges originate from  
285 the decomposition of the persulfate (KPS) initiator that will accumulate on the surface of  
286 polymer particles. On the other hand, for the dispersions prepared in the presence of MPEG, the  
287  $\zeta$ -potential value was lower (-40 to -45 mV) and close to that of neat CNC suspension. This  
288 disparity could be explained by the difference in the coverage degree of polymer particles by  
289 CNCs. In the absence of MPEG, the coverage of polymer particle is low and the surface charge  
290 is dominated by the one generated from the decomposition of KPS. The addition of MPEG as co-  
291 monomer increases the coverage degree by favoring attachment of CNCs on the surface of  
292 polymer particles, and the surface charge will be mainly dominated by the one of CNCs. These  
293 hypotheses will be supported in the following by SEM observation and rheological  
294 measurement. The beneficial effect in favoring the binding of solid particle on the polymer

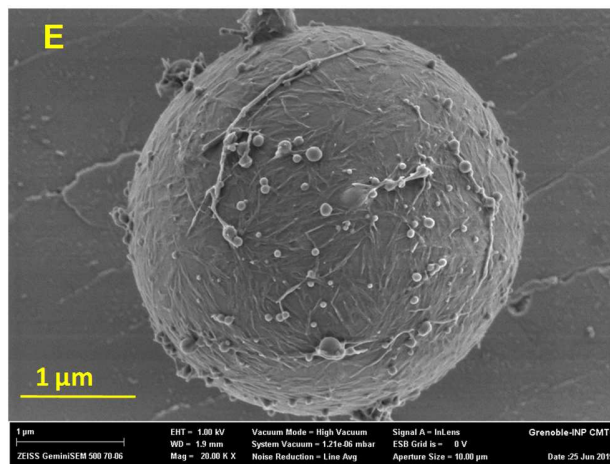
295 particle during the radical heterogenous polymerization of vinyl or acrylic monomer was also  
 296 observed for starch nanocrystals (SNCs) (Bel Haaj, Thielemans, Magnin & Boufi, 2014).



297



298



299

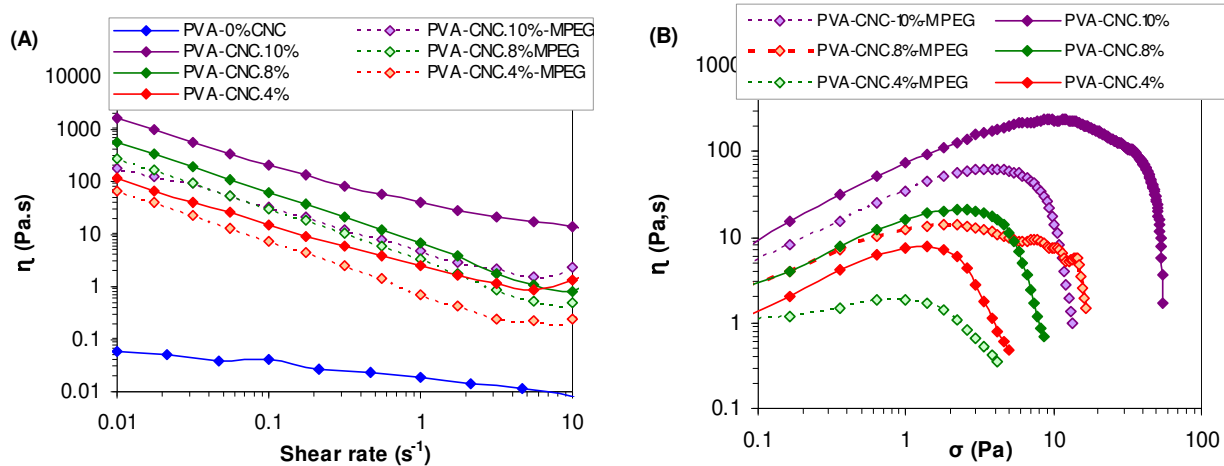
300 **Figure 3.** FE-SEM micrographs of (A,B) PVA-CNC8%, (C,D) PVA-CNC8%-MPEG, and (E)  
301 PVA-CNC-4%-MPEG dispersion produced by in-situ emulsion polymerization.

302 For PVA-CNC dispersions prepared without MPEG (Fig. 3A and 3B), FE-SEM of diluted  
303 nanocomposite dispersions dried by freeze-drying, showed well spherical polymer particles with  
304 size ranging between 100 and 300 nm. The contour of the surface of the particle is perfectly  
305 spherical and clear, which is suggestive of the lack of bound CNCs on the polymer particles.  
306 Most of the CNCs were then preferentially located in the continuous water phase being not  
307 adsorbed on the polymer particle. This hypothesis is supported by the appearance of free CNCs  
308 lying far from polymer particles as could be clearly seen in the FE-SEM observation. By  
309 contrast, in the presence of MPEG, it can be seen that the polymer particles were coated with a  
310 dense CNC layer well bound to their surface (Fig. 3C and 3D). This could be clearly seen in  
311 particle with size around 200 nm as well as for particle with large size around 2-3  $\mu\text{m}$  (Fig. 3C,  
312 3D and 3E), generated when the CNC content was 4 wt%. Interestingly, we could note on the  
313 surface the presence of tiny polymer particle with size between 20 to 100 nm adhering to  
314 polymer particle with larger size. This result might be in relation with the mechanism of particle  
315 formation during the emulsion polymerization for the CNC-MPEG system and will be discussed  
316 later.

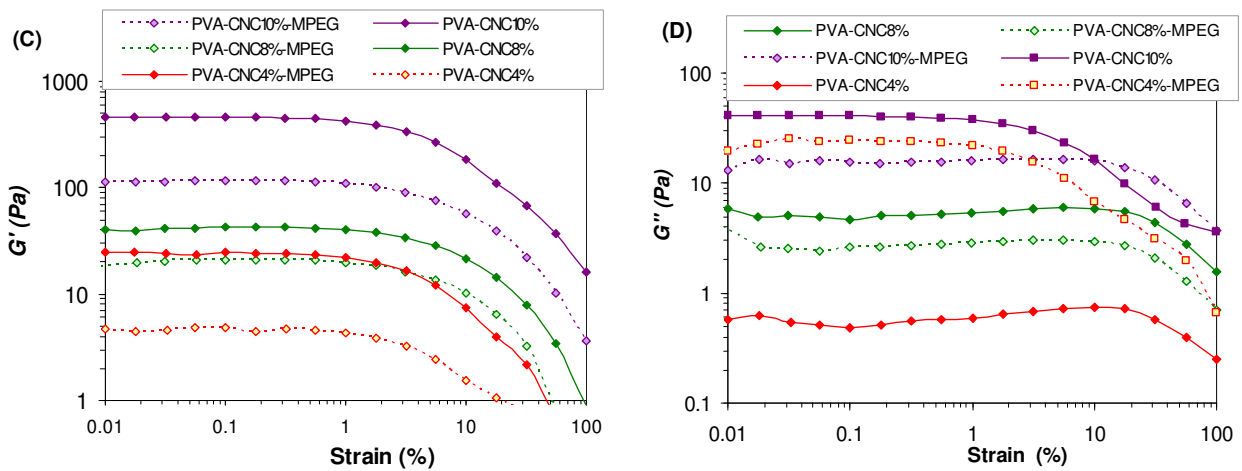
### 317 **Rheological analysis of PVA-CNCs dispersion**

318 The rheological behavior of PVA-CNC dispersions prepared via in-situ emulsion polymerization  
319 was studied in both the linear and non-linear domain by measuring the viscosity vs shear rate at  
320 different CNC contents, and the storage modulus ( $G'$ ) and loss modulus ( $G''$ ) as a function of the  
321 frequency ( $f$ ) to assess the microstructure of the nanocomposite dispersions.

322 The evolution of the viscosity versus shear rate for PVA-CNC dispersions prepared in-situ  
 323 emulsion polymerization at different CNC contents is shown in Fig. 4A. In the absence of CNCs,  
 324 the PVA dispersion, prepared under the same conditions as those adopted for PVA-CNC,  
 325 exhibited nearly a Newtonian behavior with low viscosity attaining 20 mPa.s at  $1\text{ s}^{-1}$ . In the  
 326 presence of CNCs, the viscosity of the dispersion increases by more than two decades in  
 327 comparison with the neat PVA dispersion, with an upward shift in the plot of the viscosity as the  
 328 CNC content is getting higher. For instance, the viscosity at  $1\text{ s}^{-1}$  is 2.5, 6.8 and 39 Pa.s at CNC  
 329 content of 4, 8 and 10 wt%, respectively. Moreover, the dispersion displayed a strong shear  
 330 thinning behavior as attested by the steep decrease in the viscosity as the shear rate is increasing.  
 331 When MPEG co-monomer was added during polymerization (PVA-CNC-MPEG), a lower  
 332 viscosity was reached in comparison with PVA-CNC dispersions at the same CNC content with  
 333 a depletion between 50 to 80%. (At  $1\text{ s}^{-1}$ , the viscosity attained about 0.7, 3.4 and 4.9 Pa.s).



334



335

336 **Figure 4.** (A) viscosity vs shear rate, (B) viscosity vs shear stress, (C) storage modulus ( $G'$ ) vs  
 337 strain and (D) loss modulus ( $G''$ ) vs strain for PVA-CNC dispersions at different CNC contents  
 338 and in the presence or absence of MPEG.

339 Another effect brought by the presence of CNC is the appearance of a yield stress which is  
 340 indicative of the formation of a network in PVA-SNC dispersions. Evidence of the generation of  
 341 the network structure can be seen from the plot of the shear stress ramp (Fig. 4B), revealing a  
 342 peak in the viscosity, which increased in magnitude as the CNC content increased. The peak in  
 343 viscosity represents the point at which this elastic structure breaks down resulting in shear  
 344 thinning and flow of the material. The increase in the viscosity is due to hardening of the  
 345 structure under the effect of elastic deformation below the critical strain. Except for the  
 346 composition PVA-CNC4%-MPE, all other dispersions showed a peak viscosity shifting to higher  
 347 stresses as the CNC content was increasing.

348 Another way to highlight the microstructure of PVA-CNC is to plot  $G'$  and  $G''$  as a function of  
 349 the strain at a constant angular frequency (Fig. 4C and 4D). For all PVA-CNC dispersions,  $G'$   
 350 and  $G''$  are constant up to a critical strain  $\gamma_c$  over which they steadily drop due to the collapse of  
 351 the network generated by the CNCs. With the increase in the CNC content, the magnitude of  $G'$

352 at the plateau increased substantially indicating the stiffening of the network generated by CNCs.  
353 Another remark worth to note is the higher value of  $G'$  ( $G'$  being about 8 to 10 times higher than  
354  $G''$ ), especially when the CNC content exceeds 4 wt%.

355 Based on the rheological investigation, the presence of CNCs during the emulsion  
356 polymerization of PVA generates a network imparting to the dispersion a gel-like aspect at rest.  
357 The stiffness of the network increased with the CNC content and decreased with the addition of  
358 MPEG. If we consider that in the absence of MPEG, most of CNCs are lying outside the polymer  
359 particle as evidenced by SEM observations, and then we presume that free CNCs generated a 3D  
360 network by connecting together via hydrogen bonding. This network is favored by the absence of  
361 any added surfactant and the low ionic strength of the continuous phase preventing CNCs from  
362 aggregation. The set-up of the CNC network might account for the decrease in the particle size  
363 of polymer particle as the CNC content is increasing, presumably by enclosing the polymer  
364 particle within the network reducing their coalescence during the polymerization reaction. The  
365 addition of MPEG improved the attachment of CNCs to the polymer particles during  
366 polymerization and lower fraction of CNCs remained free in water. This explain the decrease in  
367 the yield stress and  $G'$  of the dispersion along with improvement in the stabilization process  
368 (decrease in particle size) through Pickering effect induced by the binding of CNCs to the  
369 polymer particles during their growth. The preferential location of CNCs outside the polymer  
370 particle has been also recently pointed out by Ouzas et al. (Ouzas, Niinivaara, Cranston & Dubé,  
371 2018b) in the in-situ emulsion polymerization of 2-ethyl hexyl acrylate/n-butyl acrylate/methyl  
372 methacrylate without any surface modification of CNCs.

### 373 **Mechanism of emulsion polymerization in the presence of CNCs**

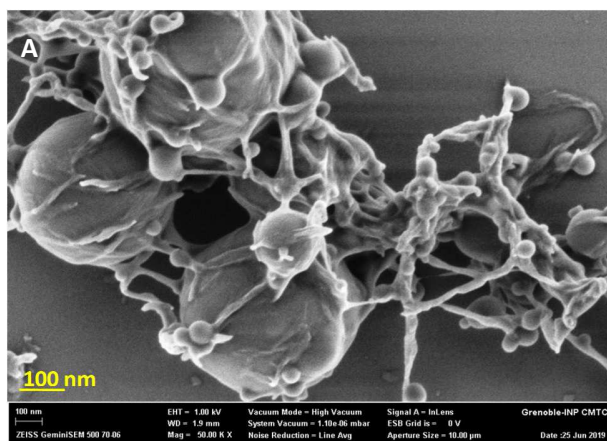
374 Based on the obtained data, we propose the following mechanism for the emulsion  
375 polymerization of VAM in the presence of CNCs. In the absence of MPEG, the polymerization

376 followed a conventional route of surfactant free emulsion polymerization, with initiation starting  
377 in the aqueous phase followed by the growth of oligo-radical until reaching a critical size to  
378 precipitate forming a nuclei that grows with monomer feeding from monomer droplets. However,  
379 given the absence of surfactant to stabilize the particle, the ensuing tiny polymer particles will  
380 aggregate one another upon choc with neighboring particles to reduce their surface and minimize  
381 their interfacial energy. By aggregation, the particles will also increase charges on their surface  
382 to reach enough zeta-potential providing enough potential barrier against the aggregation of  
383 polymer particles. The negative surface charges arise from the sulfate  $\text{SO}_4^-$  groups stemming  
384 from the decomposition of the KPS initiator.

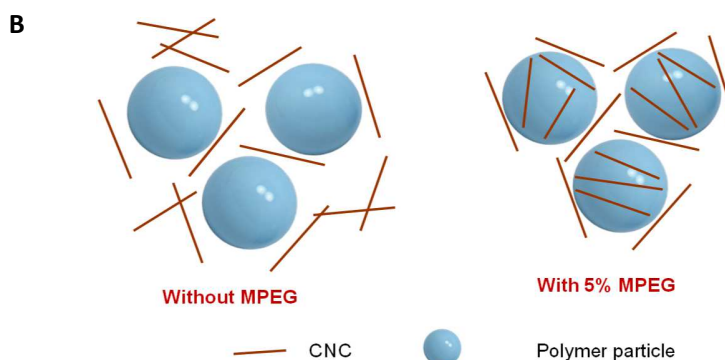
385 In the presence of CNC, the nucleation step is quite similar with generation of tiny polymer  
386 particles upon initiation in the aqueous phase and aggregation. Here again the tiny polymer  
387 particles will aggregate to reduce their surface. However, given the affinity of PEG from MPEG  
388 co-monomer with the surface of CNCs, the copolymerization of MPEG with AVM during the  
389 initiation phase will bring CNCs to the growing polymer particle and will accumulate on the  
390 surface of the particle given its hydrophilic property. As the particle grows in size, the number of  
391 CNCs bound on the polymer particle increases also until its full coverage. This hypothesis could  
392 explain the effective coating of polymer particle with CNCs when the polymerization was  
393 performed in the presence of MPEG. However, this could not explain the presence of tiny  
394 polymer particles without any attached CNC adhering to a larger polymer particle coated with  
395 CNCs. One hypothesis likely to explain this phenomenon is that a fraction of polymer particles  
396 will be generated without or with a low coverage of CNCs on their surface. These particles will  
397 agglomerate with larger polymer particles bearing CNCs.

398 The observation of the dispersion at intermediate stage of polymerization (Fig. 5A) clearly  
399 demonstrates large particles and fine particles partially coated with CNCs that are being

400 aggregated. Some tiny polymer particles were also entrapped within the CNC network. A  
401 schematic illustration of locus of CNCs depending on the presence or absence of MPEG co-  
402 monomer is depicted in Figure 5B.



403



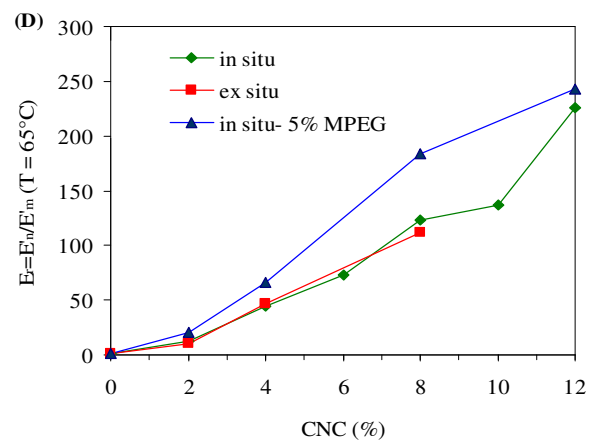
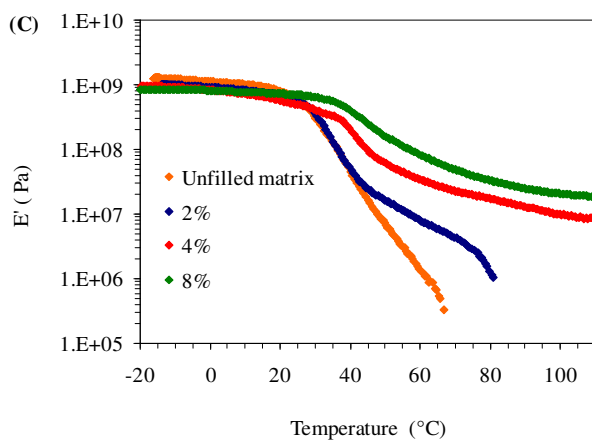
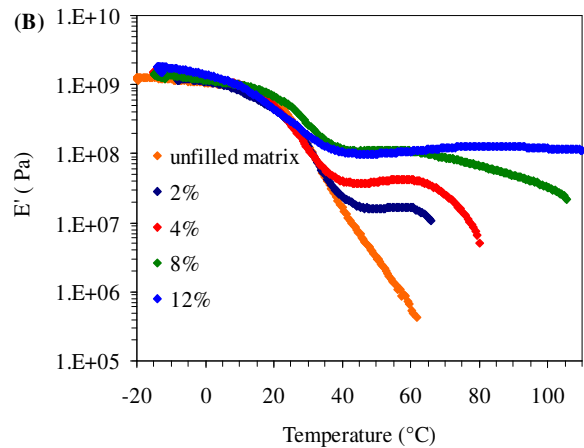
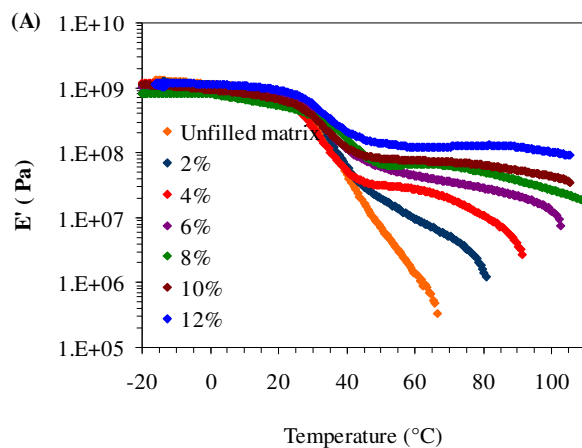
404

405 **Figure 5.** (A) FE-SEM observation of PVA-CNC6%-MPEG at about 70% conversion. (B)  
406 Schematic illustration of the locus of CNCs depending on the presence or absence of MPEG in  
407 the emulsion polymerization of VAM in the presence of CNCs.

#### 408 **Mechanical and thermal analysis of PVA-CNC nanocomposite films**

409 One of the main motivations for adding CNCs into polymer dispersion is to impart reinforcing  
410 effect to the matrix, especially when the polymer is ductile. This reinforcing effect will result in  
411 increment in the stiffness turning harder without change in its glass transition. This effect is  
412 highly desired for applications in coatings and adhesives. To investigate how the in-situ emulsion

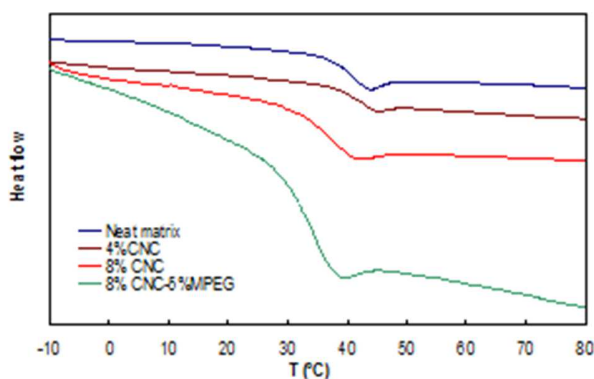
413 polymerization in the presence of the CNCs affects the reinforcing potential of nanocellulose,  
 414 nanocomposite films were prepared by simply casting the dispersion produced in-situ in a Teflon  
 415 mold and evaporating water at 45°C until complete coalescence of polymer particles and  
 416 formation of homogenous translucent films. For purpose of comparison, nanocomposite films  
 417 produced by mixing the CNC suspension with the PVA dispersion prepared by emulsion  
 418 polymerization (ex-situ route) were also prepared. The nanocomposite films were analyzed by  
 419 DMA by following the evolution of the storage modulus  $E'$  as a function of temperature over a  
 420 temperature domain spanning the glass and the rubbery domain of the polymer matrix (Fig. 6A,  
 421 6B and 6C).



424 **Figure 6.** Evolution of the storage modulus  $E'$  vs temperature for nanocomposite films from: (A)  
425 in-situ polymerization in the presence of CNC, (B) in-situ polymerization in the presence of  
426 CNC+5% MPEG, and (C) ex-situ mixing of PVA and CNC dispersion; (D) Evolution of the  
427 storage modulus as a function of CNC content at a temperature of 65°C.

428 To further highlight how the processing route affects the reinforcing potential of CNCs, the  
429 relative modulus  $E_r = E_c/E_m$  (where  $E_c$  and  $E_m$  refer to the rubbery modulus at a given  
430 temperature for the nanocomposite and the neat matrix, respectively) was plotted as a function of  
431 CNC content for films prepared by in-situ polymerization with and without MPEG and via  
432 mixing PVA dispersion with CNC suspension (Fig. 6D). For both the in-situ and ex-situ  
433 preparation route, a nearly similar trend in the modulus evolution is observed, meaning that the  
434 reinforcing effect of CNCs was not altered by the polymerization in the presence of CNC. On the  
435 other hand, when MPEG was used as co-monomer, the magnitude of the reinforcing effect was  
436 much more important in the range of CNC content between 4 and 10 wt%. For instance, at 8  
437 wt% CNC, the modulus is about 183 times higher than that of the neat matrix when MPEG was  
438 present, while the increase is only 122 and 112 times with respect to the neat matrix modulus for  
439 films prepared via in-situ polymerization and by mixing route without MPEG. One possible  
440 reason accounting for this difference might be the improvement in the binding degree of CNC to  
441 the polymer particle that prevents the risk of their aggregation during film formation process.  
442 Another reason would be the enhancement in stress transfer from the matrix to the rigid  
443 nanofiller favored by the binding of CNCs to the polymer matrix through PEG moiety.  
444 DSC analysis of nanocomposites with two different CNC contents was performed to check how  
445 the processing route might affect the  $T_g$  of nanocomposite films (Fig. 7). For the nanocomposite  
446 film with 4 wt% CNC, no evolution of the  $T_g$  was noted in comparison to neat PVA. However,

447 at 8 wt% CNC content, a depression of  $T_g$  by about 5°C and 10°C was observed for films  
448 produced in the absence and presence of MPEG, respectively. The depression observed at 8 wt%  
449 in the absence of MPEG is unexpected while that observed in the presence of MPEG is likely  
450 due to the plasticizing effect imparted by PEG chains of MPEG.

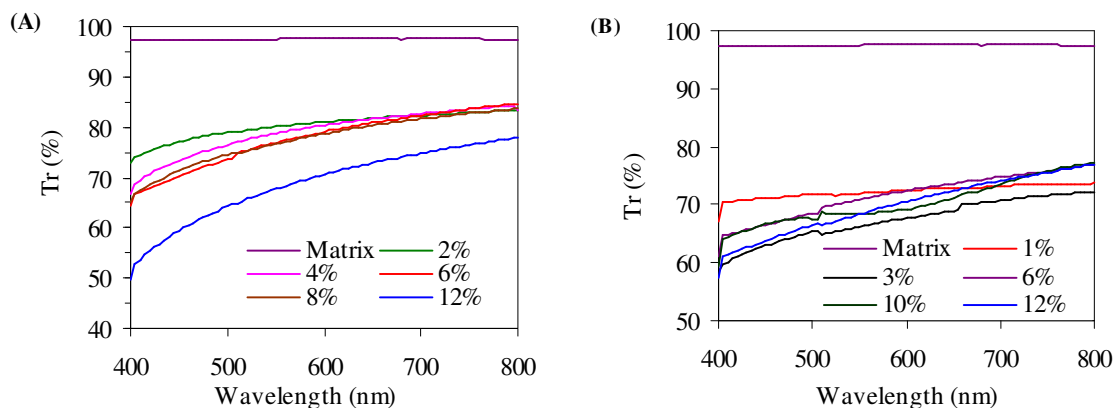


451  
452 **Figure 7.** DSC traces showing the glass transition for the neat matrix and nanocomposite films  
453 reinforced with 2, 4, and 8 wt% CNC prepared via in-situ polymerization without and with  
454 5%MPEG.

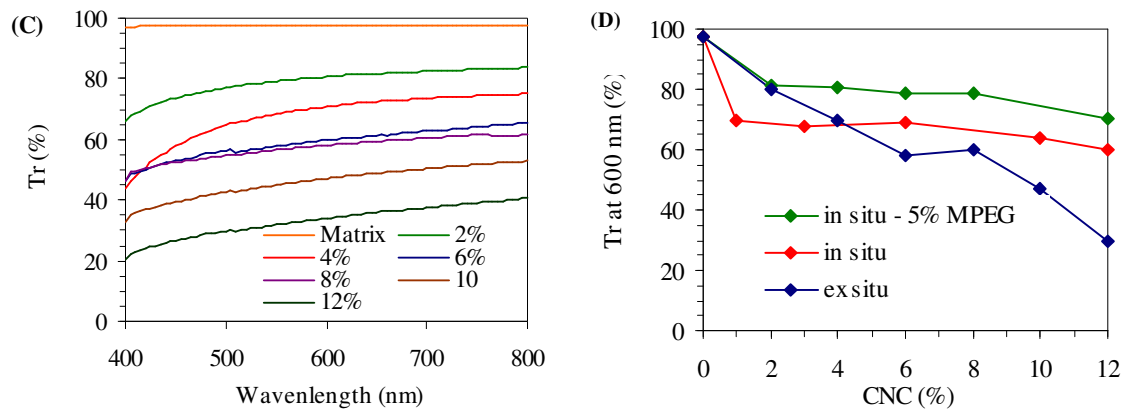
#### 455 **Transparency of PVA-CNC nanocomposites films**

456 The transparency of nanocomposite films is a simple method to assess the degree of dispersion  
457 of the nanofiller within the polymer matrix. Indeed, if we assume 40 nm as the upper limit of the  
458 nanoparticle diameter or more specifically square section, to avoid loss in the intensity of the  
459 transmitted light by scattering effect at the NP-matrix interface, then the measurement of the  
460 transmittance, normalized to a given thickness, would give an indication about the extent of CNC  
461 aggregation. The transmittance in the visible domain of nanocomposite films with different CNC  
462 contents is shown in Fig. 8. For films prepared by mixing route, a continuous decrease in the  
463 transmittance is observed as the CNC content is increased. However, the magnitude of the drop  
464 in the transmittance is less abrupt for nanocomposites prepared by the in-situ route. This could

465 be clearly discerned when the transmittance normalized with a thickness of 200  $\mu\text{m}$  is plotted vs  
466 CNC content. The transmittance degree is maintained at about 80% and 70% for films obtained  
467 by in-situ emulsion polymerization in the presence and in the absence of MPEG, respectively.  
468 This means that light scattering by CNC is much lower when the nanocomposite dispersion was  
469 produced in-situ in the presence of CNCs, especially when MPEG was present. The maintenance  
470 of the transparency over the whole CNC content range is indicative of a lack of any aggregation  
471 as the water is removed and film formation took place via coalescence of polymer particles. This  
472 feature is important for applications in coatings or adhesives where transparency of the film  
473 might be a criterious of quality. Accordingly, the production of polymer latex via emulsion  
474 polymerization in the presence of CNC would produce nanocomposite dispersions with better  
475 film quality in terms of hardness and transparency.



476

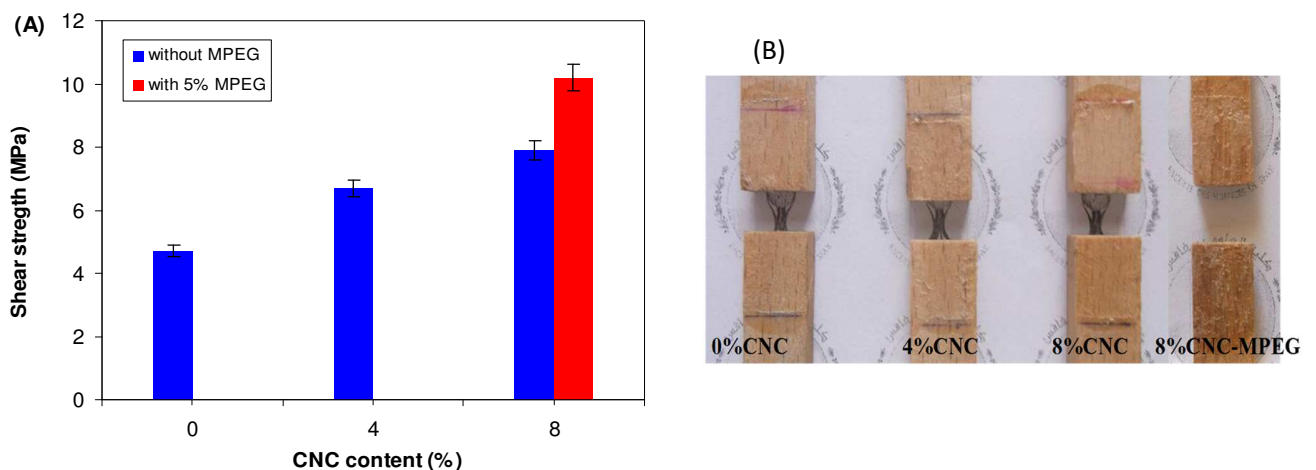


477  
 478 **Figure 8.** Transmittance for PVA-CNC nanocomposite films prepared by : (A) in-situ  
 479 polymerization in the presence of CNC, (B) in-situ polymerization in the presence of CNC+5%  
 480 MPEG, and (C) ex-situ mixing of PVA and CNC dispersion; (D) Evolution of the transmittance  
 481 at 600 nm for the different films vs CNC content.

482 **Adhesive performance produced from PVA-CNCs nanocomposite dispersion**

483 One of the widest applications of PVA dispersions is their use as main component in the  
 484 formulation of waterborne adhesives in wood industry. The good adhesion of PVA to wood and  
 485 lignocellulosic surfaces, the ease of processing of PVA adhesives, the lack of any toxicity of  
 486 PVA and the cost effectiveness of VAM are so many benefits for the widespread use of PVA in  
 487 adhesives and coatings. To show one possible interest of PVA-CNC nanocomposite dispersions  
 488 synthesized in the presence of CNCs by emulsion polymerization, wood adhesives were  
 489 formulated by simply mixing PVA-CNCs dispersions with 4 and 8 wt% CNC content, with PVA  
 490 solution. The adhesion properties of the produced adhesives were tested by producing wood  
 491 joints following standard method and the bond strength was measured using a tensile machine.  
 492 From Fig. 9A, it can be seen that the presence of CNCs led to a meaningful enhancement of the  
 493 shear strength of the joint bond, meaning that the resistance of the PVA adhesive was increased  
 494 by the presence of CNCs. For indication, the shear strength attained 4.3 MPa for unfilled PVA

495 and grows to 6.7 and about 8.4 MPa for adhesives produced from PVA-CNC containing 4 and 8  
 496 wt% CNC, respectively. This corresponds to about 155 and 195 % enhancement in the strength  
 497 in comparison with the adhesive produced from unfilled PVA. The presence of MPEG brought  
 498 further enhancement of the strength to more than 230 %, which is in agreement with DMA data,  
 499 revealing higher stiffening effect for nanocomposite films produced in the presence of MPEG.  
 500 The enhancement in adhesive performance can be seen also by observing the failure zone  
 501 showing cohesive break with detachment of wood from the specimen (Fig. 9B). This is  
 502 indicative of better penetration of the adhesive within the pore of wood and strong bonding of the  
 503 adhesive film after complete water removal and coalescence of polymer particles.



504  
 505 **Figure 9.** (A) shear strength for wood joints bonded with PVA-CNC nanocomposite adhesives  
 506 with 4 and 8 wt% CNC, and (B) photos of bonded joints after failure.

507 **CONCLUSIONS**

508 PVA dispersions were synthesized by emulsion polymerization of VAM in the presence of  
 509 CNCs using KPS/MBS as initiator without any added surfactant. Stable nanocomposite  
 510 dispersions were produced with particle size being strongly dependent on the CNC content.  
 511 MPEG co-monomer was added to promote the stabilization and further decrease the particle size

512 in the range of 200-300 nm. The addition of MPEG was shown to be effective in improving the  
513 colloidal stability of the dispersion and favoring the binding of CNCs to the surface of polymer  
514 particles. In the absence of MPEG, most of CNCs remained in the water phase without  
515 possibility of anchoring to the polymer particle. Evidence of the location of CNCs during the  
516 emulsion polymerization was confirmed by FE-SEM observations and by rheological  
517 measurements. The VAM nanocomposite dispersion led to a transparent to translucent films after  
518 casting in the form of thin films, pointing out that the presence of CNCs did not affect the film  
519 formation properties of the PVA dispersion. The reinforcing effect brought by the presence of  
520 CNCs was studied by DMA and revealed as expected a strong reinforcing effect above Tg of  
521 PVA matrix. The reinforcing effect for PVA-CNC prepared by in-situ and mixing route was  
522 quite similar. However, higher reinforcing effect was observed when the dispersion was prepared  
523 in the presence of MPEG. The transparency of the nanocomposite films was higher for films  
524 produced from PVA-CNC dispersion produced in-situ compared to those produced by mixing  
525 route. This property is beneficial for coating and adhesive applications when the transparency of  
526 the film is looked for.

## 527 **ACKNOWLEDGMENT**

528 LGP2 is part of the LabEx Tec 21 (Investissementsd'Avenir - grant agreement n°ANR-11-  
529 LABX-0030) and of the PolyNat Carnot Institut (Investissementsd'Avenir - grant agreement  
530 n°ANR-11-CARN-030-01). FE-SEM observations have been performed at CMTC  
531 characterization platform of Grenoble INP supported by the Centre of Excellence of  
532 Multifunctional Architected Materials "CEMAM" n°AN-10-LABX-44-01 funded by the  
533 "Investments for the Future" Program.

## 534 **REFERENCES**

535 Bel Haaj, S., Thielemans, W., Magnin, A., & Boufi, S. (2014). Starch nanocrystal stabilized  
536 Pickering emulsion polymerization for nanocomposites with improved performance. *ACS*  
537 *Applied Materials & Interfaces*, *6*, 8263-8273. <https://doi.org/10.1021/am501077e>.

538 Boufi, S., Kaddami, H., & Dufresne, A. (2014). Mechanical performance and transparency of  
539 nanocellulose reinforced polymer nanocomposites. *Macromolecular Materials and Engineering*,  
540 *299*, 560-568. <https://doi.org/10.1002/mame.201300232>.

541 Chaabouni, O., & Boufi, S. (2017). Cellulose nanofibrils/polyvinyl acetate nanocomposite  
542 adhesives with improved mechanical properties. *Carbohydrate Polymers*, *156*, 64-70. [https://doi:](https://doi.org/10.1016/j.carbpol.2016.09.016)  
543 [10.1016/j.carbpol.2016.09.016](https://doi.org/10.1016/j.carbpol.2016.09.016).

544 Cheng, D., Wen, Y., Wang, L., An, X., Zhu, X., & Ni, Y. (2015). Adsorption of polyethylene  
545 glycol (PEG) onto cellulose nano-crystals to improve its dispersity. *Carbohydrate Polymers*,  
546 *123*, 157-163. <https://doi.org/10.1016/j.carbpol.2015.01.035>.

547 Chern, C.S. (2006). Emulsion polymerization mechanisms and kinetics. *Progress in Polymer*  
548 *Science*, *31*, 443-486. <https://doi.org/10.1016/j.progpolymsci.2006.02.001>.

549 Dastjerdi, Z., Cranston, E.D., & Dubé, M.A. (2017). Synthesis of poly(n-butyl acrylate/methyl  
550 methacrylate)/CNC latex nanocomposites via in situ emulsion polymerization. *Macromolecular*  
551 *Reaction Engineering*, *11*, 170001. <https://doi.org/10.1002/mren.201700013>.

552 Dastjerdi, Z., Cranston, E.D., & Dubé, M.A. (2018). Pressure sensitive adhesive property  
553 modification using cellulose nanocrystals. *International Journal of Adhesion and Adhesives*, *81*,  
554 36-42. <https://doi.org/10.1016/j.ijadhadh.2017.11.009>.

555 Dufresne, A. (2017). *Nanocellulose: From Nature to High Performance Tailored Materials*, 2<sup>nd</sup>  
556 Ed., Walter de Gruyter GmbH, Berlin/Boston.

557 Eichhorn, S.J. (2012). Stiff as a board: perspectives on the crystalline modulus of cellulose. *ACS*  
558 *Macro Letters*, *1*, 1237-1239. <https://doi.org/10.1021/mz300420k>.

559 Errezma, M., Mabrouk, A.B., Magnin, A., Dufresne, A., & Boufi, S. (2018). Surfactant-free  
560 emulsion Pickering polymerization stabilized by aldehyde functionalized cellulose nanocrystals.  
561 *Carbohydrate Polymers*, 202, 621-630. <https://doi.org/10.1016/j.carbpol.2018.09.018>.  
562 <https://www.gminsights.com/industry-analysis/nanocellulose-market> (accessed 15 July 2019).

563 Kaboorani, A., Riedl, B., Blanchet, P., Fellin, M., Hosseinaei, O., & Wang, S. (2012).  
564 Nanocrystalline cellulose (NCC): a renewable nano-material for polyvinyl acetate (PVA)  
565 adhesive. *European Polymer Journal*, 48, 1829-1837.  
566 <https://doi.org/10.1016/j.eurpolymj.2012.08.008>.

567 Kalashnikova, I., Bizot, H., Bertoncini, P., Cathala, B., & Capron, I. (2013). Cellulosic nanorods  
568 of various aspect ratios for oil in water Pickering emulsions. *Soft Matter*, 9, 952-959.  
569 <https://doi.org/10.1039/C2SM26472B>.

570 Limousin, E., Ballard, N., & Asua, J.M. (2019). Synthesis of cellulose nanocrystal armored latex  
571 particles for mechanically strong nanocomposite films. *Polymer Chemistry*, 10, 1823-1831.  
572 <https://doi.org/10.1039/C8PY01785A>.

573 Mabrouk, A.B., Kaddami, H., Boufi, S., Erchiqui, F., & Dufresne, A. (2012). Cellulosic  
574 nanoparticles from alfa fibers (*Stipa tenacissima*): extraction procedures and reinforcement  
575 potential in polymer nanocomposites. *Cellulose*, 19, 843-853. [https://doi.org/10.1007/s10570-](https://doi.org/10.1007/s10570-012-9662-z)  
576 [012-9662-z](https://doi.org/10.1007/s10570-012-9662-z).

577 Kargarzadeh, H., Mariano, M., Gopakumar, D., Ahmad, I., Thomas, S., Dufresne, A., Huang, J.,  
578 & Lin, N. (2018). Advances in cellulose nanomaterials. *Cellulose*, 25, 2151-2189.  
579 <https://doi.org/10.1007/s10570-018-1723-5>.

580 O'Connor, B., Berry, R., & Goguen, R. (2014). Commercialization of cellulose nanocrystal  
581 (NCC<sup>TM</sup>) production: a business case focusing on the importance of proactive EHS

582 management. In: Hull, M., Browman, D. (Eds.) *Nanotechnology Environmental Health and*  
583 *Safety, Risks, Regulation, and Management*, 2<sup>nd</sup> Ed., Elsevier, London, pp. 225-246.

584 Ouzas, A., Niinivaara, E., Cranston, E.D., & Dubé, M.A. (2018a). Synthesis of poly(Isobutyl  
585 acrylate/n-butyl acrylate/methyl methacrylate)/CNC nanocomposites for adhesive applications  
586 via in situ semi-batch emulsion polymerization. *Polymer Composites*, 40, 1365-1377.  
587 <https://doi.org/10.1002/pc.24869>.

588 Ouzas, A., Niinivaara, E., Cranston, & E.D., Dubé, M.A. (2018b). In situ semi batch emulsion  
589 polymerization of 2-ethyl hexyl/n-butyl acrylate/methyl methacrylate/cellulose nanocrystal  
590 nanocomposites for adhesive applications. *Macromolecular Reaction Engineering*, 12, 1700068.  
591 <https://doi.org/10.1002/mren.201700068>

592 Saelices, C.J., Save, M., & Capron, I. (2019). Synthesis of latex stabilized by unmodified  
593 cellulose nanocrystals: the effect of monomers on particle size. *Polymer Chemistry*, 10, 727-737.  
594 <https://doi.org/10.1039/C8PY01575A>.

595 Saito, T., Kuramae, R., Wohler, J., Berglund, L.A., & Isogai, A. (2013). An ultrastrong  
596 nanofibrillar biomaterial: the strength of single cellulose nanofibrils revealed via sonication-  
597 induced fragmentation. *Biomacromolecules*, 14, 248-253. <https://doi.org/10.1021/bm301674e>.

598 Sheibat-Otman, N., & Bourgeat-Lami, E. (2009). Use of silica particles for the formation of  
599 organic-inorganic particles by surfactant-free emulsion polymerization. *Langmuir*, 25, 10121-  
600 10133. <https://doi.org/10.1021/la900895z>.

601 Vardanyan, V., Poaty, B., Chauve, G., Landry, V., Galstian, T., & Riedl, B. (2014). Mechanical  
602 properties of UV-waterborne varnishes reinforced by cellulose nanocrystals. *Journal of Coatings*  
603 *Technology and Research*, 11, 841-852. <https://doi.org/10.1007/s11998-014-9598-3>.

604 Vardanyan, V., Galstian, T., & Riedl, B. (2015). Effect of addition of cellulose nanocrystals to  
605 wood coatings on color changes and surface roughness due to accelerated weathering. *Journal of*  
606 *Coatings Technology and Research*, 5, 247-258. <https://doi.org/10.1007/s11998-014-9634-3>.

607 Vartiainen, J., & Vikman, M. (2013). Health and safety aspects of CNF. In: Postek, M.T., Moon,  
608 R.J., Rudie, A.W., Bilodeau, M.A. (Eds), *Production and Applications of Cellulose*  
609 *Nanomaterials*. TAPPI PRESS, GA, USA.

610 Vikman, M., Vartiainen, J., Tsitko, I., & Korhonen, P. (2015). Biodegradability and  
611 compostability of nanofibrillar cellulose-based products. *Journal of Polymers and the*  
612 *Environment*, 23, 206-215. <https://doi.org/10.1007/s10924-014-0694-3>.

613 Yu, Q., Yang, W., Wang, Q., Dong, W., Du, M., & Ma, P. (2019). Functionalization of cellulose  
614 nanocrystals with  $\gamma$ -MPS and its effect on the adhesive behavior of acrylic pressure sensitive  
615 adhesives. *Carbohydrate Polymers*, 217, 168-177. <https://doi.org/10.1016/j.carbpol.2019.04.049>.

616 Zhou, J., Li, Y., Li, H., & Yao, H. (2019). Cellulose nanocrystals/fluorinated polyacrylate soap-  
617 free emulsion prepared via RAFT-assisted Pickering emulsion polymerization. *Colloids and*  
618 *Surfaces B: Biointerfaces*, 177, 321-328. <https://doi.org/10.1016/j.colsurfb.2019.02.005>.